Photonic Effects on the Radiative Decay Rate and Luminescence Quantum Yield of Doped Nanocrystals

Tim Senden,[†] Freddy T. Rabouw,[†] and Andries Meijerink*

Condensed Matter and Interfaces, Debye Institute for Nanomaterials Science, Utrecht University, P.O. Box 80 000, 3508 TA Utrecht, The Netherlands. [†]T. Senden and F.T. Rabouw contributed equally.

ABSTRACT Nanocrystals (NCs) doped with luminescent ions form an emerging class of materials. In contrast to excitonic transitions in semiconductor NCs, the optical transitions are localized and not affected by quantum confinement. The radiative decay rates of the dopant emission in NCs are nevertheless different from their bulk analogues due to photonic effects, and also the luminescence quantum yield (QY, important for applications) is affected. In the past, different theoretical models have been proposed to describe the photonic effects for dopant emission in NCs, with little experimental validation. In this work we investigate the photonic effects on the radiative decay rate of luminescent doped NCs using 4 nm $LaPO_4$ NCs doped with Ce^{3+} or Tb^{3+} ions in different refractive index solvents and bulk crystals. We demonstrate that the measured influence of the refractive index on the radiative decay rate of the Ce^{3+} emission, having near unity QY, is in excellent agreement with the theoretical nanocrystal-cavity model. Furthermore, we show how the nanocrystal-cavity model can be used to quantify the nonunity QY of Tb^{3+}-doped $LaPO_4$ NCs and demonstrate that, as a general rule, the QY is higher in media with higher refractive index.

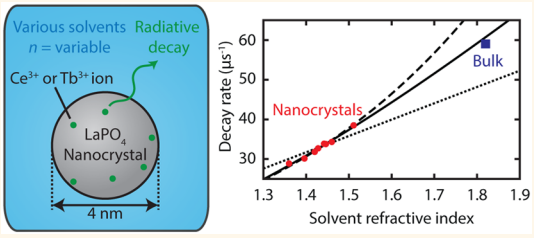

KEYWORDS: local-field effects · nanocrystals · radiative decay · luminescence quantum yield · lanthanide luminescence

Nanocrystals (NCs) doped with luminescent ions are widely investigated for application in biolabeling,[1,2] solar cells,[3] nanothermometry,[4] luminescent solar concentrators[5] or transparent luminescent media.[6] The radiative decay rate and luminescence quantum yield (QY) of the dopant ions in the NCs are important parameters for all these types of applications. For excitonic transitions in semiconductor NCs (quantum dots), the emission energy and radiative decay rate are controlled by varying the size of the NCs as these properties are influenced by quantum confinement.[7] In contrast, the optical transitions on dopant ions are localized and not affected by quantum size effects. The radiative decay rates of the dopant ions in the NCs are nevertheless different from their bulk analogues.[8] This difference originates from photonic effects as described by Fermi's golden rule and will also influence the QY of doped NCs. There has been extensive research on how the radiative decay rate of a nanoscale emitter is controlled by the photonic environment of the emitter. For example, complex photonic structures like photonic crystals[9] and plasmonic nanostructures[10] have been used to vary the local density of optical states (LDOS), to which the radiative decay rate is directly proportional. However, fundamental questions still remain even about the correct model to describe the influence of the simplest photonic environment: a homogeneous dielectric medium.[11−15]

According to Fermi's golden rule, the radiative decay rate Γ_r of an isolated electric dipole luminescent emitter in a hypothetical homogeneous dielectric medium with refractive index n is given by[14]

$$\Gamma_r(n) = \Gamma_0 n \qquad (1)$$

where n is the medium refractive index, and Γ_0 is the radiative decay rate in vacuum containing the electronic properties (transition dipole moment) of the transition. However, the dielectric surroundings of an emitter can never be truly homogeneous. For the case of doped NCs, it is evident that the NC itself constitutes a region of space with, in general, a different refractive index

* Address correspondence to a.meijerink@uu.nl.

Received for review November 25, 2014 and accepted January 13, 2015.

Published online January 13, 2015
10.1021/nn506715t

than the surrounding medium. But also if the emitter is embedded directly in a dielectric medium (*e.g.*, a dye molecule in a solvent), the dielectric surroundings are still inhomogeneous at the atomic scale. To account for these inhomogeneities, a local-field (LF) effect factor χ has to be introduced in eq 1:[16]

$$\Gamma_r(n) = \Gamma_0 n \chi^2 \quad (2)$$

The LF effect factor χ represents the ratio between the local electric field amplitude E_{loc} of photon states at the position of the emitter and the macroscopic electric field amplitude E_{mac}. According to Fermi's golden rule, it is E_{loc} that couples to the transition dipole moment of the emitter and in this manner affects the experimentally observed decay rate of an excited state.

Various theoretical models have been derived for the LF effect factor χ (for recent reviews see refs 14 and 17). The most widely applied and discussed models for χ are the full-cavity model (eq 3) and empty-cavity model (eq 4). In both models the emitter is placed in a spherical cavity inside the medium. This cavity has the size of the emitter ($d \approx$ nm) and is therefore small compared to the wavelength of the relevant photon modes ($\lambda \approx 100-1000$ nm). This is required for the quasistatic approximation to be valid.

The full- or virtual-cavity model can be applied to interstitial impurities in crystals, *i.e.*, the impurity is placed in between medium atoms. Hence, the medium around the emitter is not affected by its presence. In the corresponding cavity model, the cavity has the same refractive index as the surrounding medium. The atoms inside the cavity however do not contribute to the local electric field at the position of the emitter.[15] For this choice of cavity the radiative decay rate is described by[16]

$$\Gamma_r(n) = \Gamma_0 n \left(\frac{n^2+2}{3}\right)^2 \quad (3)$$

In contrast, the empty- or real-cavity model is used for substitutional impurities, which means that an intrinsic medium atom or molecule is replaced by an impurity. In this case, the medium is expelled from the cavity and a cavity refractive index of vacuum is assumed.[18] For this model the dependence of the radiative decay rate on the refractive index is as follows:

$$\Gamma_r(n) = \Gamma_0 n \left(\frac{3n^2}{2n^2+1}\right)^2 \quad (4)$$

It has been proposed that the LF effects for (doped) NCs in various media should be explained with an adapted case of the empty-cavity model.[17,19,20] When an emitter is situated in a NC, the NC expels intrinsic medium (solvent or glass in which the NCs are embedded) from the spherical cavity around the emitter, so the empty-cavity model should apply. The refractive index of the NC is however not 1 and has to be taken into account.[17] As a consequence, the vacuum cavity from the empty-cavity model has to be replaced by a cavity with the refractive index of the NC. This changes eq 4 to

$$\Gamma_r(n) = \Gamma_0 n \left(\frac{3n^2}{2n^2+n_{NC}^2}\right)^2 \quad (5)$$

where n_{NC} is the refractive index of the NC. This model will be further referred to as the "nanocrystal"-cavity model (NC-cavity model). As a side note, it should be mentioned that in this case a second (and constant) local field factor is hidden in Γ_0, reflecting the ratio between the electric field averaged over the volume of the NC and the field exactly at the position of the emitter.[21]

So far, experiments with doped NCs were analyzed in terms eq 3 and 4,[22−25] and therefore experimental verification of the NC-cavity model is lacking. The experiments required to verify the validity of the various LF models are challenging, as one should be able to change the dielectric medium (density of optical states) without affecting the electronic properties of the emitter (contained in the parameter Γ_0).[26] Embedding ions or molecules in a different medium usually influences the electronic ground and excited states, thus changing the transition dipole moment, and therefore Γ_0. Furthermore, for experimental access to the radiative decay rate the luminescence QY of the emitter needs to be close to 100% (or exactly known) and the decay has to be single exponential.

In this work we investigate the local-field (LF) effects (photonic effects) on the radiative decay rate for doped NCs using $LaPO_4$ doped with Ce^{3+} and Tb^{3+} ions. We compare results on doped $LaPO_4$ NCs (4 nm diameter, 15% polydispersity) in various solvents with doped bulk $LaPO_4$. For both Ce^{3+} and Tb^{3+} the electronic transitions involved are localized on the Ce^{3+} or Tb^{3+} ions and the immediate coordinating ligands. Because of the crystallinity of the host material ($LaPO_4$), the symmetry and distances to the ligands are well-defined and fixed, which ensures that the electronic states of the emitter are unaffected (Γ_0 is constant). Hence, the radiative decay rates will only be influenced by the photonic environment (refractive index), see eq 3−5. We have recently also used this system to study the photonic effects on the Förster resonance energy transfer (FRET) rate.[27]

We measure the decay dynamics of the Ce^{3+} $4f^05d^1 \rightarrow 4f^1$ transition, which is parity allowed (ns decay), and of the $Tb^{3+5}D_4 \rightarrow {}^7F_J$ transitions, which are parity forbidden (ms decay). Monoexponential decay curves are measured for the Ce^{3+}-doped NCs (QY close to unity) and it is found that the radiative decay rate of the Ce^{3+} excited state increases with increasing solvent refractive index in good agreement with the NC-cavity

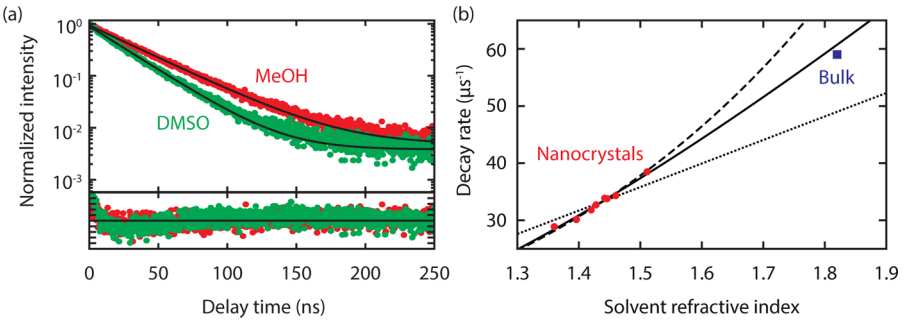

Figure 1. (a) Photoluminescence (PL) decay curves of the Ce^{3+} $4f^05d^1 \rightarrow 4f^1$ emission for $LaPO_4$:Ce^{3+} NCs dispersed in methanol (red, MeOH) and DMSO (green). Bottom panel: Fit residuals. (b) Radiative decay rates of the Ce^{3+} $4f^05d^1$ excited state for $LaPO_4$:Ce^{3+} NCs dispersed in various media (red dots) and for bulk $LaPO_4$:Ce^{3+} (blue square). The lines are fits with the full-cavity model (eq 3, dashed line), empty-cavity model (eq 4, dotted line) and NC-cavity model (eq 5, solid line, n_{NC} = 1.82).

model. In fact, the radiative lifetime of the Ce^{3+} emission in the NCs follows directly from the NC-cavity model and the Ce^{3+} emission lifetime in bulk $LaPO_4$. The Tb^{3+}-doped NCs on the other hand show multiexponential decay and decay faster than expected from the NC-cavity model and emission decay in bulk $LaPO_4$:Tb^{3+}. This is explained by nonradiative multiphonon relaxation processes for Tb^{3+} ions close to the NC surface. We use the difference between the experimental total decay rate and the decay rate based on the NC-cavity model to estimate the QY of the Tb^{3+}-doped NCs. The QY of the Tb^{3+} ions increases when a dopant-free $LaPO_4$ shell is grown around the NCs, or when they are dispersed in a solvent of higher refractive index.

RESULTS AND DISCUSSION

Ce^{3+}-Doped $LaPO_4$. Figure 1a shows photoluminescence (PL) decay curves of the Ce^{3+} emission for $LaPO_4$:Ce^{3+} NCs dispersed in methanol (MeOH) and dimethyl sulfoxide (DMSO). The decay curves were recorded for λ_{em} = 340 nm and fitted with a monoexponential function using a weighted least-squares method. The residuals in the bottom panel are random, meaning that both decay curves have a (close to) single exponential character. This indicates that the measured lifetimes are in fact radiative lifetimes, as expected, since nonradiative multiphonon relaxation from the $5d^1$ excited state will be negligible.[28] The fitted lifetimes for the $LaPO_4$:Ce^{3+} NCs dispersed in DMSO and methanol are 26 and 35 ns, respectively. Clearly, the refractive index of the solvent (photonic environment) has an influence on the decay rate. Both lifetimes are significantly longer than the lifetimes observed for bulk $LaPO_4$:Ce^{3+} (1%) ($\tau \approx$ 17 ns),[29] in agreement with eq 1−5 and the fact that n_{LaPO_4} ($n \approx$ 1.8) is higher than the refractive index of either solvent (n = 1.3−1.5).[30]

To investigate the dependence of the radiative decay rate on the refractive index, the $LaPO_4$:Ce^{3+} NCs were dispersed in several solvents, spanning a wide range of refractive indices, *i.e.*, methanol, ethanol, 1-propanol, 1-butanol, 1-pentanol, 1-hexanol, 1-octanol and DMSO (listed by order of increasing refractive index). The Ce^{3+} decay curves are single-exponential for all solvents. Since Ce^{3+} in $LaPO_4$ emits in the UV, the decay rate depends on the solvent refractive index in the UV, which deviates slightly from well-known values in the visible. To determine the refractive index in the UV of the various solvents, we used a home-built setup to measure the critical angle of total internal reflection of a UV laser beam at the quartz glass/solvent interface (λ = 325 nm, close to the maximum of the Ce^{3+} emission in $LaPO_4$). Typically, the refractive index at 325 nm was 0.03 higher than the n_D^{20} values reported for the solvents[31] (see Methods). In Figure 1b the radiative decay rates of the Ce^{3+} $4f^05d^1$ excited state (red dots, average over five measurements) are plotted as a function of the solvent refractive index. The standard deviation over the five measurements is within the size of the symbols in Figure 1b.

Besides the Ce^{3+}-doped $LaPO_4$ NCs, we use bulk $LaPO_4$:Ce^{3+} for studying the photonic effects on the radiative decay rate, as this can be regarded as $LaPO_4$:Ce^{3+} NCs in a medium of $LaPO_4$. We find a radiative lifetime of 17 ns for the Ce^{3+} $4f^05d^1$ excited state of bulk $LaPO_4$:Ce^{3+} (blue square in Figure 1b), which is in good agreement with previously reported lifetimes.[29,32] The refractive index n_{LaPO_4} was estimated at 1.82, 0.03 higher than the reported n_D^{20} value of 1.79,[30] in analogy with the increase of 0.03 in refractive index observed for the different solvents when going to the UV.

In order to determine which theoretical model can explain the trend in our experimental results, we fitted the data points of the NCs to the full-cavity model (eq 3, dashed line), empty-cavity model (eq 4, dotted line) and nanocrystal-cavity (NC-cavity) model (eq 5, solid line, n_{NC} = 1.82), as is shown in Figure 1b. Comparison of the experimental results with the three models for the different solvents shows that both the full-cavity model and the NC-cavity model can explain the increase in radiative decay rate of the Ce^{3+} emission in the solvents (for n = 1.36−1.51). The empty-cavity

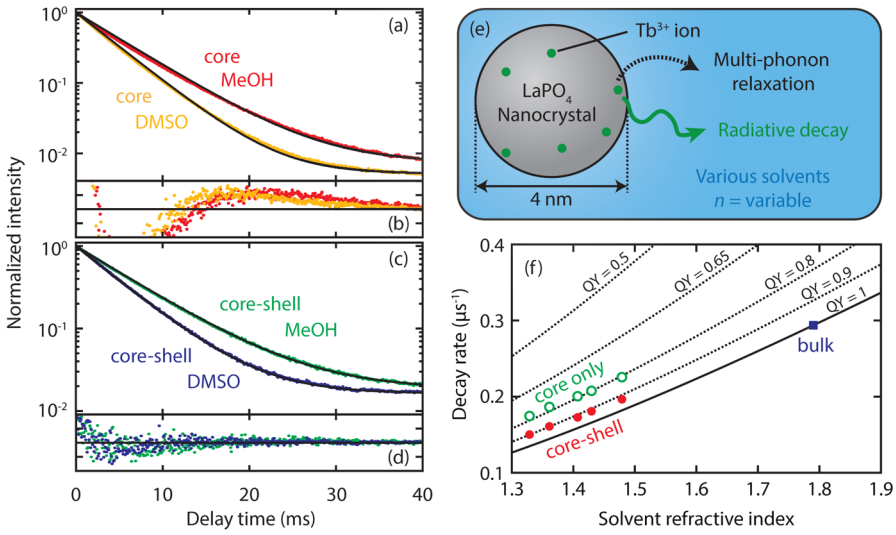

Figure 2. PL decay properties of $LaPO_4$:Tb^{3+} NCs (core) and $LaPO_4$:Tb^{3+}/$LaPO_4$ NCs (core−shell). (a and c) PL decay curves of the Tb^{3+} $^5D_4$ excited state for core NCs (a) and core−shell NCs (c) dispersed in methanol (MeOH) and DMSO. (b and d) Fit residuals for core NCs (b) and core−shell NCs (d). (e) Schematic image of a Tb^{3+}-doped $LaPO_4$ NC in solution. The Tb^{3+} ions on or close to the NC surface can lose their excitation energy through radiative decay or multiphonon relaxation. (f) Decay rates of the Tb^{3+} $^5D_4$ state as a function of the solvent refractive index. Experimental data: core NCs (green, open dots), core−shell NCs (red, filled dots) and bulk $LaPO_4$:Tb^{3+} (blue square). The solid line gives the expected total decay rates for $LaPO_4$:Tb^{3+} NCs in case QY = 1, which are radiative decay rates obtained using the NC-cavity model. The dotted lines give the expected total decay rates for $LaPO_4$:Tb^{3+} NCs with a QY lower than 1, which are obtained by adding a nonradiative contribution.

model clearly underestimates the influence of the refractive index on the radiative decay rate. The radiative decay rate observed for the Ce^{3+} emission in bulk $LaPO_4$ allows to distinguish between the full- and NC-cavity model and shows that the NC-cavity model is the only model that can explain the variation in decay rate over the full range of refractive indices (n = 1.36−1.82). The present result provides evidence that the NC-cavity model (eq 5) is valid for doped NCs in dielectric media. Not only can the model explain the variation in decay rate as a function of the refractive index of surrounding media, it also allows the determination of the radiative decay rate for emission from dopants in NCs from the refractive index of the dielectric medium and the radiative decay rate in the bulk material. In the next section we will explore this feature and demonstrate how it can be applied to estimate nonradiative decay rates for dopants in NCs.

Tb^{3+}-Doped $LaPO_4$. Figure 2 shows PL decay curves of the Tb^{3+} emission for (a) $LaPO_4$:Tb^{3+} NCs and (c) $LaPO_4$:Tb^{3+}/$LaPO_4$ core−shell NCs with a ∼1 nm thick dopant-free shell of $LaPO_4$, dispersed in methanol and DMSO. The decay curves were recorded at λ_{em} = 540 nm in the $^5D_4 \rightarrow {}^7F_5$ transition and weighted least-squares fitted with a monoexponential function. The fit residuals of each curve are shown in the panels (b) and (d) below the decay curves. The residuals in panel (b) indicate that the decay of the Tb^{3+} emission for the $LaPO_4$:Tb^{3+} NCs (core only) is not single exponential. The initial faster decay is caused by the competition between radiative decay and nonradiative decay processes for Tb^{3+} ions located on or close to the NC surface,[33,34] as illustrated in Figure 2e. Nonradiative decay occurs *via* multiphonon relaxation to high energy phonons of ligand molecules. Both C−H and N−H vibrations of ∼3000 cm^{-1} can contribute to multiphonon relaxation. The energy gap between the emitting $^5D_4$ and the next lower $^7F_0$ level is ∼13000 cm^{-1}. This gap can be bridged by five high energy phonons of the ligands. The energy gap law for lanthanide emission states that in case of an energy gap of fewer than five phonons, nonradiative multiphonon decay can compete with radiative decay.[16,35] Note that in bulk $LaPO_4$, with a maximum phonon energy of ∼1200 cm^{-1} (phosphate vibrations),[35] the gap requires more than 10 phonons and multiphonon relaxation rates will be negligibly small. As a result, the observed decay rate for the $^5D_4$ emission in bulk $LaPO_4$ corresponds to the radiative decay rate.

The fit residuals for the Tb^{3+} emission decay curves recorded for the core−shell NCs, shown in Figure 2d, indicate that the fast nonradiative component is significantly reduced when a $LaPO_4$ shell is grown around the original $LaPO_4$:Tb^{3+} NCs, which results in a close to single exponential decay curve. The undoped $LaPO_4$ shell increases the distance between Tb^{3+} ions in the NCs and the high energy vibrations of surface ligands, which strongly reduces the multiphonon relaxation due to these ligands. This is consistent with the results of Kömpe *et al.*, who measured that the QY of $CePO_4$:Tb^{3+}/$LaPO_4$ NCs increases to 70% after shell growth (QY was below 50% for the original $CePO_4$:Tb^{3+} core NCs).[34]

Figure 2f shows single-exponential fitted decay rates of the Tb^{3+} $^5D_4$ state (average over five

measurements) as a function of the solvent refractive index. Both the results of the core NCs (green, open dots) and core−shell NCs (red, filled dots) are displayed. The standard deviation is within the size of the symbols in Figure 2f. The solvents used were methanol, ethanol, tetrahydrofuran, 1-octanol and DMSO, with refractive indices taken from ref 31 (λ = 589 nm). We synthesized bulk $LaPO_4:Tb^{3+}$ (1%) and measured a radiative lifetime of 3.4 ms for the $^5D_4$ excited state (indicated by blue square in Figure 2f). This value is in good agreement with previous reported $^5D_4$ emission lifetimes for Tb^{3+} in bulk $LaPO_4$.[29,32] In Figure 2f we use this bulk lifetime to determine the radiative decay rates (solid line) expected for the Tb^{3+} emission of the NCs dispersed in solvents with varying refractive index *n*, based on the NC-cavity model (eq 5), where we assume that the $^5D_4$ state in bulk LaPO4:Tb^{3+} (1%) has a unity QY.[35] It is observed that the decay of Tb^{3+} excited state of the doped NCs (green and red symbols) is faster than what is expected from the NC-cavity model. This difference is due to multiphonon relaxation in the NCs (Figure 2e), which is suppressed but not fully eliminated when a dopant-free $LaPO_4$ shell is grown (compare green symbols to red symbols).

Photoluminescence Quantum Yield of Doped NCs. The NC-cavity model yields the radiative decay rate of dopants in NCs, as was shown for $LaPO_4:Ce^{3+}$ (see Figure 1). If the dopant transition has a unity QY, as in the case of $LaPO_4:Ce^{3+}$ NCs, the radiative decay rate is equal to the total decay rate measured in the experiment. However, now in the case of Tb^{3+}, nonradiative multiphonon relaxation contributes to the total decay rate. Hence, we will show that the NC-cavity model can be used to estimate this nonradiative contribution and thereby provide the PL QY of the Tb^{3+}-doped NCs. Note that this method will provide an upper limit for the PL QY of doped NCs, namely the PL QY of only the emissive dopant ions in the ensemble. In contrast to conventional methods quantifying absorption and emission, it is insensitive to ions that absorb but are otherwise completely dark, *e.g.*, those situated next to a quenching center.[36] Consequently, our method can yield larger ensemble QY values (disregarding the ions with a QY of zero) than conventional methods which average over all ions. Interestingly, from the difference between values obtained with the two methods one can in principle calculate the fraction of dark ions.

In Figure 2f, the dotted lines show expected total decay rates for $LaPO_4:Tb^{3+}$ NCs with a QY lower than 1, which were obtained using the NC-cavity model to determine the radiative decay rate and adding a nonradiative decay contribution. It can be seen that the QYs of the $LaPO_4:Tb^{3+}$ core-only NCs and the $LaPO_4:Tb^{3+}/LaPO_4$ core−shell NCs are approximately 0.8 and 0.9, respectively. It is interesting that the QY at low refractive index (n = 1.33) is slightly lower than at higher refractive index (n = 1.48). This indicates that the

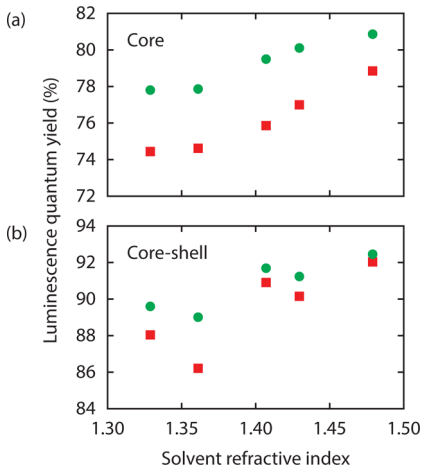

Figure 3. Luminescence QY of (a) $LaPO_4:Tb^{3+}$ core-only NCs and (b) $LaPO_4:Tb^{3+}/LaPO_4$ core−shell NCs as a function of the solvent refractive index. The luminescence QY was calculated using either the fitted lifetimes from Figure 2f (green dots) or integrating the area under the experimental decay curves for the NCs in the various solvents (red squares).

QY of the NCs increases with increasing refractive index. To further investigate this, we calculated the QY of the core and core−shell NCs in the various solvents using the total decay rates from Figure 2f and the expected radiative decay rates according to the NC-cavity model. Figure 3 shows the QY (green dots) of (a) the $LaPO_4:Tb^{3+}$ core-only NCs and (b) the $LaPO_4:Tb^{3+}/LaPO_4$ core−shell NCs using this method. A clear trend is visible that the QY of the NCs increases with increasing refractive index. This is expected if we assume that the nonradiative decay rate is constant, while we know that the radiative decay rate increases with increasing refractive index. The trend that the QY of a doped NC increases if the refractive index of the solvent increases, is general as long as the solvent itself does not provide nonradiative decay channels (nonradiative decay only due to surface ligands).

For the $LaPO_4:Tb^{3+}$ NCs in this work, with a QY close to unity, it was possible to fit the PL decay to a monoexponential function (Figure 2a and 2c) and use the method of Figure 2f to determine the QY. A more accurate and generally applicable method (also for more strongly multiexponential decay curves) to determine the QY is not fitting the luminescence decay curve, but integrating the area under the curve. Figure 4 shows PL decay curves (blue solid lines) of (a) $LaPO_4:Tb^{3+}$ NCs and (b) $LaPO_4:Tb^{3+}/LaPO_4$ core−shell NCs in methanol. The area under these decay curves (blue) is a measure for the total number of emitted photons by the NCs (background subtracted). Furthermore, Figure 4 displays single exponential PL decay curves (red dashed lines) based on the radiative decay rate predicted the NC-cavity model. The area under these curves represents the number of photons emitted by the NCs if the QY were unity. The difference between the two areas (red) is the loss due to

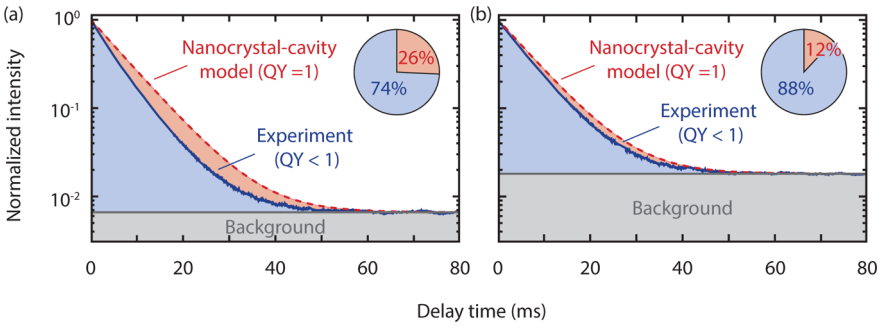

Figure 4. Determination of the luminescence QY of Tb^{3+}-doped NCs *via* integration of area under decay curves. The panels show measured PL decay curves (blue) of (a) $LaPO_4$:Tb^{3+} NCs and (b) $LaPO_4$:Tb^{3+}/$LaPO_4$ core−shell NCs in methanol (n = 1.33). The red dashed lines are simulated decay curves for $LaPO_4$:Tb^{3+} NCs for the case of a unity QY. The simulated PL decay curves were obtained using the NC-cavity model for QY = 1 and n = 1.33. The QY of the NCs (pie chart in top right corner of panels) is determined by integrating the area under the experimental decay curve (blue area) and simulated PL decay curve for QY = 1. The difference between the two curves gives the nonradiative decay (red area).

nonradiative decay. Hence the relative areas of red and blue directly provide us with the average QY of the sample, which is illustrated by the pie chart in the top right corner of each panel. We obtain an upper limit for the QY of 74% for the $LaPO_4$:Tb^{3+} NCs in methanol and a QY of 88% for the $LaPO_4$:Tb^{3+}/$LaPO_4$ core−shell NCs in methanol.

Figure 3 shows the QY of the NCs determined using this integration method for all solvents (red squares). It can be seen that the QY increases with increasing refractive index, which agrees with the results for the lifetimes obtained from fits to a monoexponential function (green circles). The QY values of the integration technique are however lower than those obtained with the fitted lifetimes of Figure 2f. This is due to the fact that the integration technique is better at taking into account a full distribution of decay rates, and therefore more accurately determines the nonradiative decay component. As a result, the difference in QY between the two methods is larger for the core-only NCs, for which the decay curves were more multiexponential compared to the core−shell NCs.

To obtain these absolute values for the QY of the $LaPO_4$:Tb^{3+} NCs, we have used the radiative lifetime of the bulk counterpart, directly measured from a bulk sample with near-unity QY. If in a more general case a bulk sample with near-unity QY is not available, the total lifetime (including nonradiative contributions) of a bulk sample can be used. Our method would then, however, yield the QY ratio between NCs and bulk rather than the absolute QY of the NCs.

Influence of NC Shape and Size on NC-Cavity Model. The NC-cavity model assumes that the NCs are spherical, but NCs are rarely perfectly spherical. To illustrate that the NC-cavity model is also good for NCs with deviating shape, we consider the case of ellipsoidal NCs for which analytical models exist.[14,37] The local-field (LF) effect factor χ in ellipsoidal NCs depends on the polarization of the emitter with respect to the long axis. If we compare a spherical NC (4 nm $LaPO_4$ in methanol) to

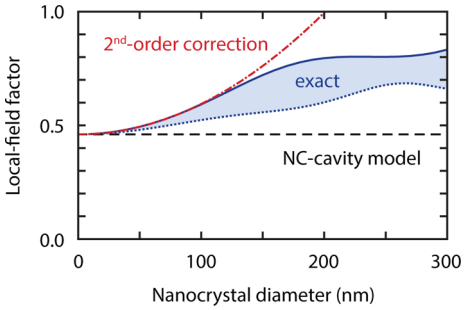

Figure 5. Theoretical local-field (LF) effect factor for doped $LaPO_4$ NCs (n_{NC} = 1.79) in methanol (n = 1.33) as a function of the NC size. Exact calculations of the LF factor following ref 38 are shown for dopants in the center of the NC (blue solid line) and at the surface (blue dotted line). The exact calculations are compared to the LF factor according the NC-cavity model (eq 5, black dashed line) and the NC-cavity model including a second-order correction (eq 6, red dot-dashed line).

an ellipsoidal NC of equal volume but with an aspect ratio as large as 10, the orientationally averaged radiative lifetime of dopants would be no more than 7% shorter in the ellipsoid. Hence, small deviations of the shape of NCs from perfectly spherical can safely be ignored in the NC-cavity model.

The NC-cavity model further assumes that NCs are very small with respect to the wavelength of the emitted light. More precisely, it is valid in the limit that $ka \ll 1$, where $k = 2\pi/\lambda$ is the free space wave vector of the emitted light and a is the radius of the NC. In our case of NCs with a diameter of 4 nm emitting (primarily) at 540 nm this requirement is easily met: ka = 0.02. Figure 5 shows the theoretical LF factor for larger $LaPO_4$ NCs (n_{NC} = 1.79) in methanol (n = 1.33), for dopants in the center (blue solid line) and at the surface (blue dotted line).[38] Most importantly, we see that for small NCs of a few nm in diameter the exact size does not affect the LF factor, and the NC-cavity model (black dashed line) is very accurate. In somewhat larger NCs the biggest deviation between the exact calculations and the NC-cavity model is for dopants at the center. For these we can

obtain a second-order correction to the NC-cavity model (red dot-dashed line), by expanding the expressions from ref 38 for small *ka*:

$$\Gamma_r(n) = \Gamma_0 n \left(\frac{3n^2}{2n^2 + n_{NC}^2}\right)^2 \left[1 + \frac{(n_{NC}^2 - n^2)(n_{NC}^2 + 10n^2)}{5(2n^2 + n_{NC}^2)}(ka)^2\right] \quad (6)$$

The NC-cavity model is accurate to within 5% if the second term between square brackets in eq 6 is smaller than 0.05. For $LaPO_4$:Tb^{3+} in methanol this is for NCs smaller than 41 nm in diameter. We conclude that (depending on the refractive indices involved, the emission wavelength and the desired accuracy) the NC-cavity model is reliable for NCs with sizes of up to several tens of nm.

CONCLUSIONS

The decay dynamics of the Ce^{3+} $5d^1$ and Tb^{3+} $^5D_4$ excited state have been studied for Ce^{3+} or Tb^{3+} ions in $LaPO_4$ nanocrystals (NCs) and bulk material. We analyzed the influence of the photonic environment on the radiative decay rate by measuring luminescence decay curves of the Ce^{3+} and Tb^{3+} emission for 4 nm $LaPO_4$ NCs in solvents of different refractive index (n = 1.3–1.5). For the $5d^1$ emission of Ce^{3+} single exponential decay curves are observed, showing an increase in radiative decay rate with n in excellent agreement with the theoretical NC-cavity model. In addition to establishing the validity of the NC-cavity model, it allows an accurate determination of the radiative lifetime for dopant emission in NCs in a solvent with refractive index n using the radiative lifetime in bulk material. Furthermore, we have shown how an upper limit of the luminescence QY can be determined for Tb^{3+}-doped $LaPO_4$ NCs in solution by comparison of the nonexponential luminescence decay curves and the radiative decay rate (from the NC-cavity model and bulk emission lifetime). The results showed that the QY of the Tb^{3+} emission in doped $LaPO_4$ NCs increases when a dopant-free shell is grown and when the refractive index of the solvent is higher.

Photonic (local field) effects will be present in all applications of luminescent doped NCs. The results presented in this work will be important for future applications of doped NCs in *e.g.*, biolabeling, solar cells and transparent luminescent materials. The method presented to determine the QY and radiative decay rate of luminescent doped NCs using the NC-cavity model will be of great significance for the field nanomaterials science.

METHODS

Synthesis and Characterization of Doped $LaPO_4$ NCs. Ce^{3+} or Tb^{3+}-doped $LaPO_4$ NCs were synthesized following refs 34 and 39. Briefly, a clear solution of 10 mmol of (hydrated) lanthanide chlorides in 10 mL of methanol was mixed with 40 mmol of diethyl ethylphosphonate (Ce^{3+}-doped NCs) or tributyl phosphate (Tb^{3+}-doped NCs). The methanol was evaporated under a vacuum at room temperature on a Schlenk line, after which 30 mL of diphenyl ether was added to the solution. Subsequently, water was removed from the solution under a vacuum on a Schlenk line by heating to 100 °C, and 40 mmol of tributylamine and 7 mL of a 2 M solution of phosphoric acid in dihexyl ether were added to the solution. Next, the reaction mixture was heated at 200 °C under nitrogen atmosphere for approximately 18 h, during which the NCs were formed. The NCs were isolated from the crude reaction mixture by centrifugation, washed with toluene and dried under a vacuum.

For the synthesis of the core–shell NCs,[34] 7.0 mL of a 2 M solution of phosphoric acid in dihexyl ether was added to the crude reaction mixture (no isolation and purification of core NCs). The reaction mixture was then stirred vigorously and heated to 200 °C. Separately, a solution of $LaCl_3 \cdot 6H_2O$ (10 mmol) in 10 mL of methanol was mixed with 40 mmol of tributyl phosphate. After the methanol and water had been removed from the solution as described above (heating to 100 °C under a vacuum), the solution was mixed with 40 mmol of tributylamine and subsequently added to the reaction mixture (2 mL solution added every 5 min). The reaction mixture was then kept at 200 °C under nitrogen atmosphere for approximately 18 h. The core–shell NCs were isolated from the reaction mixture in the same way as the core NCs.

Transmission electron microscopy images showed that monodisperse NCs with a diameter of 4 nm were obtained. The diameter of the NCs increased to 6 nm when a dopant-free $LaPO_4$ shell was grown. Powder X-ray diffraction measurements confirmed that the crystal structure of the NCs was in agreement with the monoclinic monazite phase of $LaPO_4$. Inductively coupled plasma atomic emission spectroscopy (ICP-OES) was used to determine that the $LaPO_4$ NCs were doped with 0.9% Ce^{3+} or Tb^{3+} ions.

The synthesized tributylamine capped NCs could easily be redispersed in polar organic solvents for photoluminescence (PL) measurements, and all prepared solutions were stable and clear. The solvents used were methanol, ethanol, 1-propanol, 1-butanol, 1-pentanol, 1-hexanol, 1-octanol, tetrahydrofuran (THF) and dimethyl sulfoxide (DMSO). In PL measurements, only dilute colloidal solutions were used (10 mg of NCs in 3 mL of solvent) to prevent the influence of reabsorption effects.

Synthesis of Bulk Doped $LaPO_4$. The synthesis of microcrystalline $LaPO_4$:Ce^{3+}(1%) or $LaPO_4$:Tb^{3+}(1%) was based on a method described by Van Schaik *et al.*[32] Stoichiometric amounts of La_2O_3 (9.9 mmmol), $(NH_4)_2HPO_4$ (20 mmol) and CeO_2 (0.2 mmol) or Tb_4O_7 (0.05 mmol) were mixed and grinded with a pestle in an agate mortar and subsequently fired in air at 900 °C for 3 h. After an intermediate grinding, a second firing was carried out in a reducing atmosphere (10%/90% H_2/N_2) at 1200 °C for 3 h. A white powder was obtained. X-ray diffraction measurements confirmed that the crystal structure of the obtained powders was in agreement with the monoclinic monazite phase of $LaPO_4$. No second crystal phase was observed.

Photoluminescence Measurements. Photoluminescence (PL) spectra and decay curves were measured using an Edinburgh Instruments FLS920 fluorescence spectrometer. A PicoQuant pulsed diode laser (λ_{ex} = 270 nm, repetition rate 2.5 MHz, pulse width 650 ps) was used for excitation of the Ce^{3+} ions. PL spectra and decay curves of the Ce^{3+} emission were recorded with a fast Hamamatsu H74220–60 photomultiplier tube (PMT). The decay curves were obtained using time-correlated single photon counting with an Edinburgh TCC900 computer card. Excitation of the Tb^{3+} ions was done with an optical parametric oscillator (OPO) system (Opotek HE 355 II) pumped by the third harmonic of a Nd:YAG laser. The OPO system was set at λ_{ex} = 486 nm to excite in the Tb^{3+} $^7F_6 \rightarrow {}^5D_4$ f–f transition (repetition rate 10 Hz, pulse width 10 ns). PL spectra and decay curves of the Tb^{3+} emission were recorded with a Hamamatsu R928 PMT detector. The decay curves

were obtained using the multichannel scaling (MCS) option integrated in the FLS920 fluorescence spectrometer.

Refractive Index Measurement. To obtain the refractive index in the UV of the different solvents, we used a home-built setup to measure the critical angle of total internal reflection of a UV laser beam (Kimmon He/Cd IK3151R-E; λ = 325 nm) on the quartz/solvent interface. We found refractive indices of 1.36 for methanol, 1.40 for ethanol, 1.42 for 1-propanol, 1.43 for 1-butanol, 1.44 for 1-pentanol, 1.45 for 1-hexanol, 1.46 for 1-octanol and 1.51 for DMSO.

Conflict of Interest: The authors declare no competing financial interest.

Acknowledgment. We gratefully acknowledge H. Siekman and P. de Graaf for building the setup required to measure the refractive index in the UV. This work is part of the research program of the "Stichting voor Fundamenteel Onderzoek der Materie (FOM)", which is financially supported by the "Nederlandse Organisatie voor Wetenschappelijk Onderzoek (NWO)".

REFERENCES AND NOTES

1. Diamente, P. R.; van Veggel, F. C. J. M. Water-Soluble Ln^{3+}-Doped LaF_3 Nanoparticles: Retention of Strong Luminescence and Potential as Bio-Labels. *J. Fluoresc.* **2005**, *15*, 543–551.
2. Heer, S.; Kömpe, K.; Güdel, H.-U.; Haase, M. Highly Efficient Multicolour Upconversion Emission in Transparent Colloids of Lanthanide-Doped $NaYF_4$ Nanocrystals. *Adv. Mater.* **2004**, *16*, 2102–2105.
3. Wang, G.; Peng, Q.; Li, Y. Lanthanide-Doped Nanocrystals: Synthesis, Optical-Magnetic Properties, and Applications. *Acc. Chem. Res.* **2011**, *44*, 322–332.
4. Jaque, D.; Vetrone, F. Luminescence Nanothermometry. *Nanoscale* **2012**, *4*, 4301–4326.
5. Erickson, C. S.; Bradshaw, L. R.; McDowall, S.; Gilbertson, J. D.; Gamelin, D. R.; Patrick, D. L. Zero-Reabsorption Doped-Nanocrystal Luminescent Solar Concentrators. *ACS Nano* **2014**, *8*, 3461–3467.
6. Zharkouskaya, A.; Feldmann, C.; Trampert, K.; Heering, W.; Lemmer, U. Ionic Liquid Based Approach to Luminescent $LaPO_4$:Ce,Tb Nanocrystals: Synthesis, Characterization and Application. *Eur. J. Inorg. Chem.* **2008**, *2008*, 873–877.
7. Alivisatos, A. P. Semiconductor Clusters, Nanocrystals, and Quantum Dots. *Science* **1996**, *271*, 933–937.
8. Meltzer, R.; Yen, W.; Zheng, H.; Feofilov, S.; Dejneka, M.; Tissue, B.; Yuan, H. Effect of the Matrix on the Radiative Lifetimes of Rare Earth Doped Nanoparticles Embedded in Matrices. *J. Lumin.* **2001**, *94*−*95*, 217–220.
9. Lodahl, P.; Van Driel, A. F.; Nikolaev, I. S.; Irman, A.; Overgaag, K.; Vanmaekelbergh, D.; Vos, W. L. Controlling the Dynamics of Spontaneous Emission from Quantum Dots by Photonic Crystals. *Nature* **2004**, *430*, 654–657.
10. Frimmer, M.; Koenderink, A. F. Spontaneous Emission Control in a Tunable Hybrid Photonic System. *Phys. Rev. Lett.* **2013**, *110*, 217405.
11. Purcell, E. M. Spontaneous Emission Probabilities at Radio Frequencies. *Phys. Rev.* **1946**, *69*, 681.
12. Drexhage, K. Influence of a Dielectric Interface on Fluorescence Decay Time. *J. Lumin.* **1970**, *1*−*2*, 693–701.
13. Schuurmans, F.; de Lang, D.; Wegdam, G.; Sprik, R.; Lagendijk, A. Local-Field Effects on Spontaneous Emission in a Dense Supercritical Gas. *Phys. Rev. Lett.* **1998**, *80*, 5077–5080.
14. Toptygin, D. Effects of the Solvent Refractive Index and Its Dispersion on the Radiative Decay Rate and Extinction Coefficient of a Fluorescent Solute. *J. Fluoresc.* **2003**, *13*, 201–219.
15. Wuister, S. F.; de Mello Donega, C.; Meijerink, A. Local-Field Effects on the Spontaneous Emission Rate of CdTe and CdSe Quantum Dots in Dielectric Media. *J. Chem. Phys.* **2004**, *121*, 4310–4315.
16. Henderson, B.; Imbusch, G. F. *Optical Spectroscopy of Inorganic Solids*; Clarendon Press: Oxford, 1989; pp 146−157.
17. Duan, C. K.; Reid, M. F. Macroscopic Models for the Radiative Relaxation Lifetime of Luminescent Centers Embedded in Surrounding Media. *Spectrosc. Lett.* **2007**, *40*, 237–246.
18. Glauber, R.; Lewenstein, M. Quantum Optics of Dielectric Media. *Phys. Rev. A: At., Mol., Opt. Phys.* **1991**, *43*, 467–491.
19. Liu, H.; Guyot-Sionnest, P. Photoluminescence Lifetime of Lead Selenide Colloidal Quantum Dots. *J. Phys. Chem. C* **2010**, *114*, 14860–14863.
20. Hens, Z.; Moreels, I. Light Absorption by Colloidal Semiconductor Quantum Dots. *J. Mater. Chem.* **2012**, *22*, 10406–10415.
21. Pukhov, K. K.; Basiev, T. T.; Orlovskii, Y. V. Spontaneous Emission in Dielectric Nanoparticles. *JETP Lett.* **2008**, *88*, 12–18.
22. Meltzer, R.; Feofilov, S.; Tissue, B.; Yuan, H. Dependence of Fluorescence Lifetimes of Y_2O_3:Eu^{3+} Nanoparticles on the Surrounding Medium. *Phys. Rev. B: Condens. Matter Mater. Phys.* **1999**, *60*, R14012–R14015.
23. Dolgaleva, K.; Boyd, R. W.; Milonni, P. W. Influence of Local-Field Effects on the Radiative Lifetime of Liquid Suspensions of Nd:YAG Nanoparticles. *J. Opt. Soc. Am. B* **2007**, *24*, 516–521.
24. He, E.; Zheng, H.; Zhang, X.; Qu, S. Local-Field Effect on the Fluorescence Relaxation of Tm^{3+}:LaF_3 Nanocrystals Immersed in Liquid Medium. *Luminescence* **2010**, *25*, 66–70.
25. Xue, X.; Suzuki, T.; Tong, H. T.; Ohishi, Y. Investigation of Local Field Effect of α-$NaYF_4$:Nd^{3+} Nanocrystals. *Phys. Status Solidi* **2012**, *9*, 2481–2484.
26. Schuurmans, F. J. P.; Lagendijk, A. Luminescence of $Eu(fod)_3$ in a Homologic Series of Simple Alcohols. *J. Chem. Phys.* **2000**, *113*, 3310–3314.
27. Rabouw, F. T.; den Hartog, S. A.; Senden, T.; Meijerink, A. Photonic Effects on the Förster Resonance Energy Transfer Efficiency. *Nat. Commun.* **2014**, *5*, 3610.
28. Dorenbos, P. 5d-Level Energies of Ce^{3+} and the Crystalline Environment. III. Oxides Containing Ionic Complexes. *Phys. Rev. B: Condens. Matter Mater. Phys.* **2001**, *64*, 125117.
29. Bourcet, J.-C. Quantum Efficiency of Diffusion Limited Energy Transfer in $La_{1-x-y}Ce_xTb_yPO_4$. *J. Chem. Phys.* **1974**, *60*, 34–39.
30. Weber, M. J. *Handbook of Optical Materials*; CRC Press: Boca Raton, FL, 2002.
31. Haynes, W. M. *Handbook of Chemistry and Physics*, 94th ed.; CRC Press: Boca Raton, FL, 2011.
32. Schaik, W. V.; Lizzo, S.; Smit, W.; Blasse, G. Influence of Impurities on the Luminescence Quantum Efficiency of (La, Ce, Tb)PO_4. *J. Electrochem. Soc.* **1993**, *140*, 216–222.
33. Riwotzki, K.; Meyssamy, H.; Schnablegger, H.; Kornowski, A.; Haase, M. Liquid-Phase Synthesis of Colloids and Redispersible Powders of Strongly Luminescing $LaPO_4$:Ce,Tb Nanocrystals. *Angew. Chem., Int. Ed.* **2001**, *40*, 573–576.
34. Kömpe, K.; Borchert, H.; Storz, J.; Lobo, A.; Adam, S.; Möller, T.; Haase, M. Green-Emitting $CePO_4$:Tb/$LaPO_4$ Core-Shell Nanoparticles with 70% Photoluminescence Quantum Yield. *Angew. Chem., Int. Ed. Engl.* **2003**, *42*, 5513–5516.
35. Blasse, G.; Grabmaier, B. C. *Luminescent Materials*; Springer-Verlag: Heidelberg, 1994.
36. Würth, C.; Geißler, D.; Behnke, T.; Kaiser, M.; Resch-Genger, U. Critical Review of the Determination of Photoluminescence Quantum Yields of Luminescent Reporters. *Anal. Bioanal. Chem.* **2014**, *407*, 59–78.
37. Pukhov, K. K.; Basiev, T. T. Radiative Transitions in Nanocrystals. *Opt. Mater.* **2010**, *32*, 1664–1667.
38. Dung, H.; Knöll, L.; Welsch, D.-G. Spontaneous Decay in the Presence of Dispersing and Absorbing Bodies: General Theory and Application to a Spherical Cavity. *Phys. Rev. A: At., Mol., Opt. Phys.* **2000**, *62*, 053804.
39. Oertel, A.; Lengler, C.; Walther, T.; Haase, M. Photonic Properties of Inverse Opals Fabricated from Lanthanide-Doped $LaPO_4$ Nanocrystals. *Chem. Mater.* **2009**, *21*, 3883–3888.